



Flame Spread Transition to Regression of Thick Fuel in Oxygen-Limited Concurrent Flow

Feng Zhu, Key Laboratory of Microgravity, Institute of Mechanics, Chinese Academy of Sciences, Beijing 100190, China

Xinyan Huang, Research Center for Fire Safety Engineering, The Hong Kong Polytechnic University, Hong Kong, China*

Xiao Chen, State Key Laboratory of Fire Science, University of Science and Technology of China, Hefei, China

Shuangfeng Wang, Key Laboratory of Microgravity, Institute of Mechanics, Chinese Academy of Sciences, Beijing 100190, China, State Key Laboratory of High-Temperature Gas Dynamics, Chinese Academy of Sciences, Beijing, China and School of Engineering Science, University of Chinese Academy of Sciences, Beijing, China*

Received: 4 June 2022/**Accepted:** 9 January 2023/**Published online:** 27 January 2023

Abstract. The flame behaviors in a narrow gap with low-velocity airflow are significantly different from buoyancy-controlled flames in open areas. The conditions experienced by microgravity flame may be reproduced in a narrow gap environment where the buoyancy is limited. This work studies the behaviors of near-limit concurrent flame spread over a thick solid fuel in an oxygen-limited narrow channel with 3 mm and 5 mm heights. As the concurrent airflow and oxygen concentration decrease below a critical value, the flame spread transitions to the fuel-regression mode, burning like a candle flame. Further reducing the oxygen, the flame tip tilts towards the inflow like the flame in the opposed flow. A flammability map is found to define three regimes (1) concurrent flame spread, (2) fuel regression, and (3) extinction. The fuel-regression regime is characterized by a fuel regression angle of over 30° and a global flame equivalence ratio of over 1.9. The existence of the fuel-regression mode extends the low-flow flammability limit in the concurrent flow. The ‘round-trip’ flame phenomenon is observed where the 1st-stage near-limit opposed flame spread transitions to the 2nd-stage fuel regression in the concurrent flow. This work provides new insights into the concurrent flame-spread and extinction behavior under oxygen-limited and microgravity environments.

Keywords: Fire spread, Near-limit, Fuel regression, Flammability, Flamelet, Thick PMMA

*Correspondence should be addressed to: Xinyan Huang, E-mail: xy.huang@polyu.edu.hk; Shuangfeng Wang, E-mail: sfwang@imech.ac.cn



1. Introduction

The concurrent flame spread is dominated by convective heat transfer from the flame to the solid fuel, which is much faster than the opposed spread flame [1, 2]. There is a series of research on concurrent flame spreading over solid fuels (e.g. [3, 4]), and the influence factors of oxygen concentration [5, 6], gas flow [7–10], ambient pressure [11] have been studied in unconfined space. The flammability test method based on upward spread flame has been widely used in the selection of material in spacecraft and aircraft design [12–14]. However, there are some conditions where the oxygen supply is limited, such as in small gaps or regions where materials are in close proximity, such as inside a wall or between folds of cloth on the ground, as well as in microgravity spacecraft environments. From the perspective of fire prevention, it is imperative to give an insight into the concurrent flame spread over solid fuel under a limited oxygen supply.

Under normal gravity, the concurrent flame spread over thermally-thick solid fuel with varied flow velocities has been systematically studied [5, 15]. The flame spread rate increases with the concurrent flow velocity before blowoff, and both the flame spread rate and burning rate can reach a steady state. At low oxygen concentration, a “surface” flame spread may occur where the fuel is not burnt out after the flame spreads over. A similar process is found in a PMMA rod in microgravity, where the flame oscillates by flashing forward upstream and retreating downstream [16, 17]. For a thick solid, the steady-state concurrent flame spread is also observed in the microgravity and oxygen-limited environment [18–20].

For a concurrent spreading flame, it is a diffusive flame in nature, and all pyrolyzed fuel gases will be burnt in flame at a near-unity equivalence ratio. As the oxygen supply is limited, the global stoichiometry increases. Then, flame spread behavior becomes significantly different from that in an environment with rich oxygen. The buoyant flow suppressed environment is one of the typical oxygen supply limit conditions, and the narrow-channel type apparatus has been widely used to suppress buoyancy that can capture the essential features of microgravity flame spread over both thin and thick solid fuel [9, 21–27]. When the channel height is lowered to a critical value and/or the flow velocity is reduced to a critical value, excessive pyrolyzed fuel accumulates at the flame leading edge, and the system becomes fuel-rich [24]. Recent microgravity experiments [28, 29] revealed that, for ultra-thin solid fuels, when the airflow rate was low enough, there is an opposed-flame structure due to flow recirculation or oxygen diffusion.

The quenching limit and instabilities of opposed flame spread over thermally-thick solid fuel have been experimentally studied in microgravity [30] and narrow-channel environments [9, 27, 31–33]. The uniform flame cannot be sustained under a low flow velocity, so the flamelets or fingering phenomena will be formed. The diffusive-thermal instability of a thin solid is probably the trigger force. The near-limit flame spread behavior for thin solid fuel has been studied, and two kinds of instabilities have been identified, namely fingering or cellular type and traveling wave instability [34]. For the concurrent flame spread over thick solid fuel, past research has focused on the spread process under sufficient buoyancy flow [11, 20, 35], while the near-limit flame spread requires further research.

The present paper investigates the flame-spread behaviors over thermally thick solid fuel with the low-velocity concurrent flow in a horizontal narrow channel apparatus. The effect of external gas flow velocity on concurrent flame spread behavior is experimentally examined. A new flammability map for different flame modes as a function of the concurrent flow velocity and oxygen concentration is presented. Then, the controlling mechanisms of different flame spread modes are discussed, and the global flame equivalence ratio is analyzed to quantify the influence of the overall oxygen supply.

2. Experimental Method

The schematic of the experimental setup is shown in Figure 1. The narrow channel is 164 mm wide, 410 mm long. The channel height (H) are 3 and 5 mm, which are narrow enough to suppress the buoyant flow velocity [21]. The inlet of the channel is filled with gauze to prevent the convergence of the two jets, and then an aluminum honeycomb to ensure a uniform gas flow. The ambient atmosphere was O_2/N_2 mixtures. During each test, the air was supplied from the compressor, and the 18.1% O_2/N_2 mixtures were supplied from the gas bottle. Other ambient atmospheres were achieved by mixing air with N_2 or O_2 . The gas flow velocity and oxygen concentration were controlled by two mass flow controllers (Alicat Scientific, type MC) which allowed the mixture with a prescribed oxygen concentration between 15% and 30% at flow velocity from 0 cm/s to 20 cm/s. The flow velocity and oxygen concentration were measured using a hot-wire anemometer and a fuel gas analyzer (TESTO 350) at the outlet of the flow tunnel, respectively (see Figure 1). Typical velocity profiles are provided in Figure 12. For visualization purposes, the top and side walls of the channel are made of quartz glass.

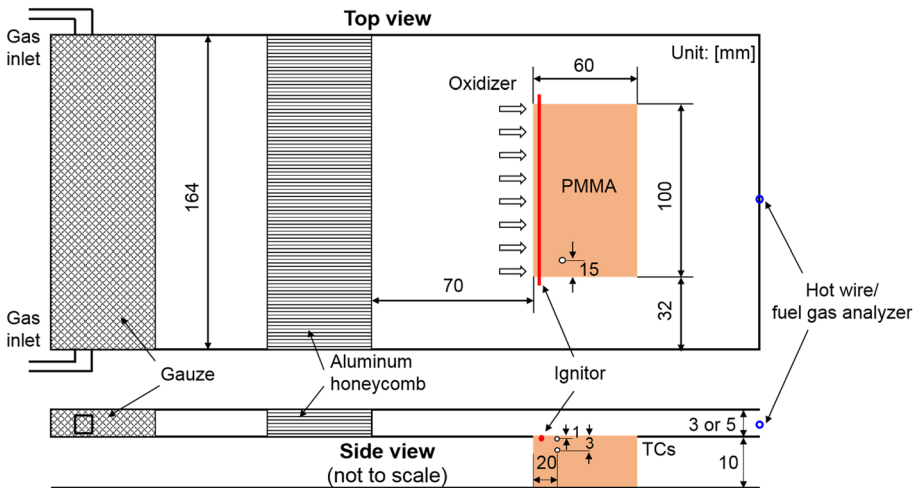


Figure 1. Schematic of the experimental setup, where all dimensions are in millimeters (not to scale).

The fuel used in the experiments is a 10 mm thick polymethylmethacrylate (PMMA) plate, measuring 60 mm long by 100 mm wide. The sample is wide enough to study the effect of the flame spread behavior near the extinction limit. The position of the sample is shown in Figure 1, where it is 70 mm far away from the flow outlet along the center of the channel. The fuel sample is embedded in the aluminum floor of the test section, with its top face flushed with the floor and the side and bottom faces insulated from the sample holder. Ignition is accomplished by energizing a resistively heated wire, and the ignition wire is embedded 1.5 mm from the upstream end. The fuel sample is ignited with a power of 116 W. Two thermocouples (type-K, 0.075 mm in diameter) are used for temperature measurement.

As shown in Figure 1, these thermocouples are positioned 1 mm and 3 mm beneath the surface, 20 mm downstream, and 15 mm from one side because of the difficulty in drilling a hole with a diameter of 0.5 mm. Pyrolysis occurs when the temperature is reached 350 °C, so the regression rate is calculated. Note that with the regression of the sample, the channel height will be increased. The flow profile inside the channel will be changed, and the flame spread process will be influenced inevitably. This work focuses on the pyrolysis front spread rate, the regression rate, and the flame spread mode. During each experiment, if the spread rate of the pyrolysis front is constant, the influence of the channel height variation can be neglected.

Flame spread behaviors at 21% and 18.1% O₂ with flow velocities in the range of 0 ~ 20 cm/s were studied. Then the flammability boundary was measured under oxygen concentrations in the range of 15% to 30%. In this work, the flame spread rate was defined as the propagate rate of the pyrolysis front in accordance with Loh and Fernandez-Pello [5] and Jiang et al. [36]. When the flame spread rate is tested, a white LED is used to illuminate the fuel sample, and the flame spread behaviors are recorded by a Sony DCR-TRV900E with a resolution of 1440 by 1080 pixels at 25 fps from the top view. While the flame base is recorded, a black background is provided. Another digital video camera (Nikon D7200, 25 fps) with a resolution of 1920 by 1080 pixels was set to record the burning and extinction process from the side-top (45°) view. The camera settings were adjusted to record the flame spread for different test cases since the flame luminosities vary significantly.

The flammability map was obtained as following: at a specified oxygen concentration, the sample was ignited with a relatively large flow velocity (e.g. 4 cm/s under 25% O₂, 10 cm/s under 21% O₂, 12 cm/s under 18% O₂), then the flow velocity was decreased by 1 cm/s at a 60-s interval. To ensure the experimental repeatability, all tests were repeated at least three times. The relative error of oxygen concentration was about ± 0.2%. The precision of the gas flow velocities in the forced flow experiments was about ± 5%. The uncertainty of measured flame spread rate was mainly due to the ambiguity of the pyrolysis front.

3. Results

3.1. Flame Spread and Burning Behaviors

Figure 2 shows flame images captured from side-top (45°) view during the flame spread processes in concurrent flow of (a) 20.9% (air) and (b) 18.1% O_2 concentrations (see Videos S1 and S2). These images were taken during the steady-state flame spread at the corresponding gas flow velocities. Under a sufficient concurrent airflow of 4 cm/s, the flame is pushed forward and inclined toward the unburnt solid surface, as illustrated in Figure 3a. Therefore, the flame can effectively heat the downstream fuel surface above the pyrolysis point and cause a ‘continuously piloted ignition’, that is, a typical concurrent flame spread [1, 18]. In addition, a yellow flame tail is formed, indicating that there is adequate oxygen supply to the flame.

As the airflow reduces to 3 cm/s, the flame length reduces, and the yellow flame disappears, indicating that the oxygen supply becomes limited. Further reducing

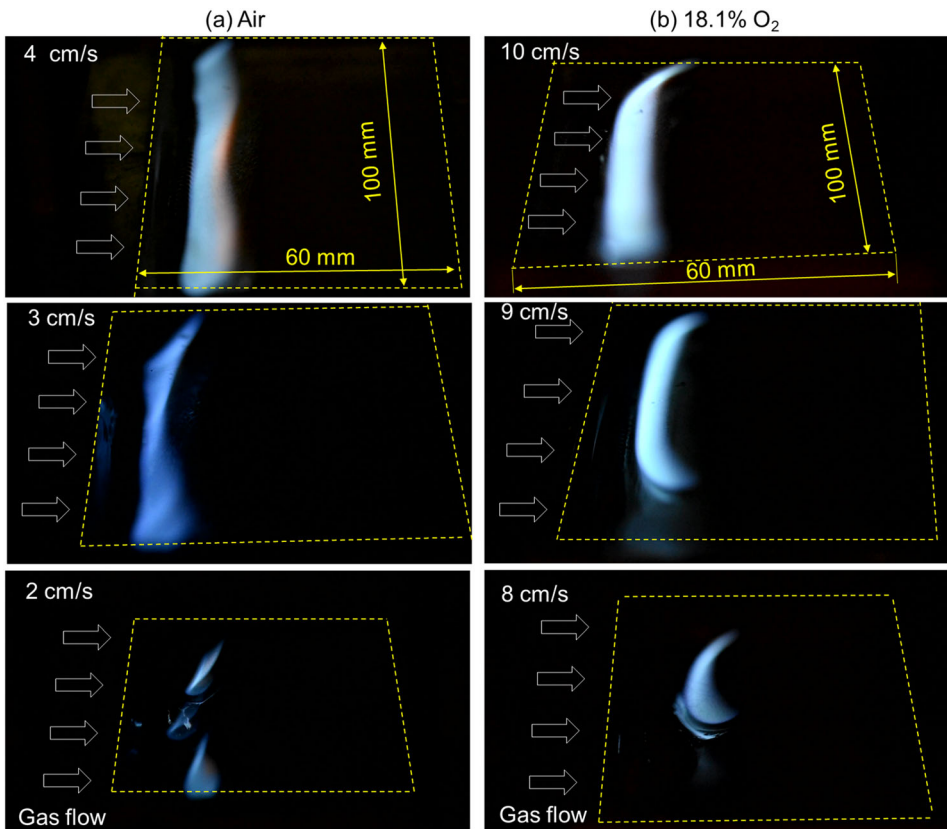


Figure 2. Flame images (side-top view) during the steady-state spread at different concurrent flow velocities in (a) air and (b) 18.1% O_2 (see Videos S1 and S2).

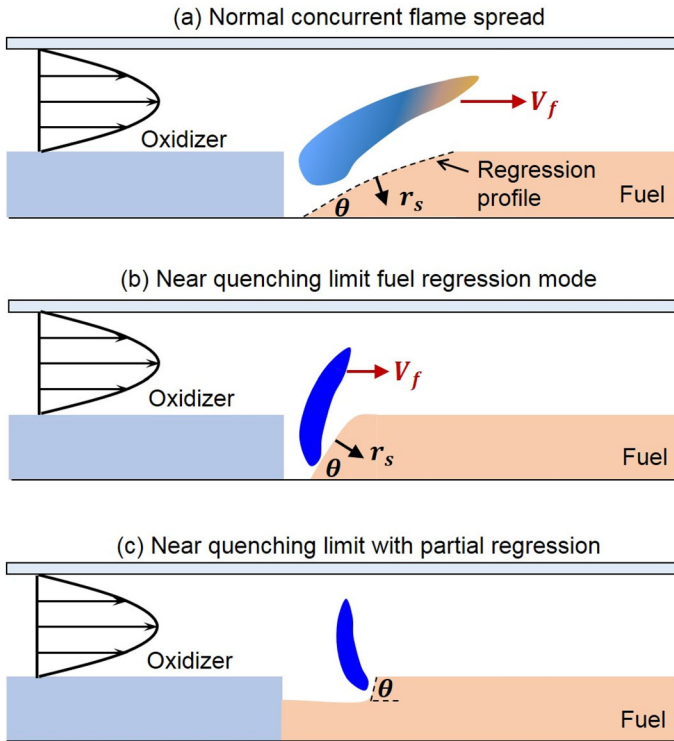


Figure 3. Schematic diagram of (a) normal concurrent flame spread, (b) near-limit fuel-regression mode, and (c) partial regression near-extinction.

the airflow to 2 cm/s, the uniform flame front cannot be sustained after the ignition; instead, it breaks into three small flamelets, forming a fingering pattern, as shown in Figure 2a. The side view shows that the flame is almost standing up, as illustrated in Figure 3b. The flame length is nearly constant, as the tail of the flame did not move forward. The flame moves forward only when the fuel under the flame base is completely consumed, so that the concurrent flame spread (continuously piloted ignition) transitions to the fuel-regression mode. Such a process is similar to the motion of a candle flame, where the flame moves due to the regression of wax. Note that this fuel-regression mode is stable that can last for more than 30 min until the burnout of the entire fuel. A similar transition to a stable fuel-regression mode was also observed previously in the opposed flame spread near the blowoff limit [37].

Similar processes also occur at 18.1% O₂ condition (Figure 2b), where the uniform flame cannot be sustained at a concurrent flow velocity below 10 cm/s. As the flow velocity further decreases, the flame front shrinks into a single flamelet rather than breaking into multiple flamelets, so it is also a typical flamelet mode

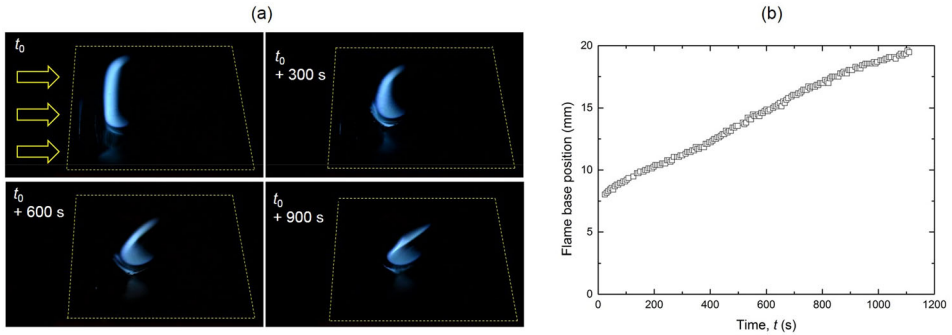


Figure 4. (a) Flame behaviors on PMMA under 18.1% O_2 with a concurrent flow velocity of 8 cm/s (see Video S2), and (b) the time evolution of the flame base position.

[30, 32, 33]. Figure 4 shows a more detailed evolution of this single flamelet, which is stable enough to last for over 20 min.

Previously, the separation and shrinkage of a uniform flame front have been observed in microgravity experiments [30] and the narrow channel apparatus [9, 32]. The near quenching limit instabilities of concurrent flame spread over thin solid fuel have been studied [34], and two kinds of instabilities have been identified, namely fingering or cellular type and traveling wave instability. For a concurrent flame spread over a thick solid fuel, flamelet only occurs in the Fuel-Regression Regime. Similar to the opposed spread flame, near extinction, the lack of oxygen supply weakens the flame and the associated flame heating, so the three-dimensional diffusion effects become strong [23, 38–40].

Moreover, the flame is tilted more towards upstream and against the flow, when the oxygen supply is extremely lacking. Then, the flame spreads downstream instead of anchoring on the base of the fuel, as illustrated in Figure 3c. At the same time, the regression is limited in the burning zone and only a thin surface layer of PMMA forms before extinction (i.e., partial regression). In other words, the overall cooling from the environment and thick fuel prevent the burnout of PMMA in-depth directly, and similar phenomena were also observed in the narrow-channel fingering spread with pure oxygen [32]. The evolution of the flame base position as a function of time is shown in Figure 4b. See more details about the flame from top-view in the Appendix. It is likely that if the sample fuel is long enough, the flame base will continuously propagate downstream. For a sample with a small length, the flame may finally be extinguished at the end of the fuel sample, because the opposed flame cannot be sustained under this condition. The partial regression mode is defined by the time evolution of the flame base position.

3.2. Flammability Map

Figure 5a summarizes the flammability map in terms of oxygen concentration and concurrent flow velocity for a 5 mm gap spacing near the low-flow extinction limit. Typically, under sufficient oxygen supply, the flame spreads forward along

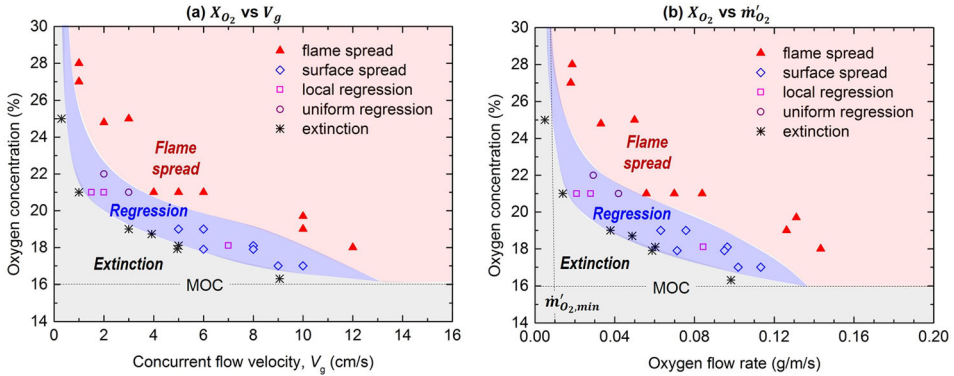


Figure 5. Flammability maps for concurrent flame spread in a 5-mm narrow channel environment, (a) oxygen level vs. flow velocity, and (b) oxygen level vs. oxygen flow rate.

with the oxidizer flow and regresses in depth. As the oxygen concentration or flow velocity decreases, eventually, extinction occurs due to a lack of oxygen supply. Nevertheless, there is an extra *Fuel-Regression Regime* between the Flame-Spread Regime and Extinction Regime, where the flame is stable and robust. Here, both the regression mode (Figure 3b) and partial regression mode (Figure 3b) are defined as regression mode, for the reason that the flame length and pyrolysis length is almost constant.

Note that such a Fuel-Regression Regime was not observed previously in the 10-mm gap channel [9]. In contrast, the fuel-regression mode also occurs in the 3-mm narrow channel experiment. Thus, the lack of buoyancy flow is a key factor for this fuel-regression regime, which is expected to occur in a microgravity environment as well. In particular, the fuel-regression mode is easy to occur in the low-velocity flow of high oxygen concentration ($> 25\%$) because the flame becomes more intensive. Comparatively, the fuel-regression regime is narrow in the low-oxygen flow, and it eventually disappears when approaching PMMA's minimum oxygen concentration (MOC) of 16% [41]. Two boundaries merge because the flame becomes weak in low oxygen concentration, and increasing the flow velocity can easily blow off the flame.

Previous studies [9, 42] show that when the oxygen supply is quite limited, the flame is more persistent (or more difficult to extinguish) in the concurrent oxidizer flow than in the opposed flow, because the flaming heating in the concurrent flow is more effective. The transition to the fuel-regression mode will further extend the flammability map of "concurrent" flame spread (see more discussion in Sect. 4).

Note that the flammability map of Figure 5a is affected by the height of the narrow channel. In a channel with a large gap, the flammability range becomes wider. Thus, Figure 5b further plots the flammability map in terms of oxygen concentration and the linear oxygen mass flow rate ($\rho_g V_g H Y_{O_2}$) in the narrow channel. A similar tendency is observed where the limit oxygen concentrations (LOCs) of both the flame spread and fuel regression decrease with the increased oxygen

flow rate, and eventually, two boundaries merge at $MOC = 16\%$. Moreover, there is a minimum oxygen mass flow rate of 0.01 g/m/s for flame spread, which is also observed in the previous 10-mm channel experiments [9].

3.3. Rates of Flame Spread and Fuel Regression

Well above the extinction limit, the flame spreads forward, and the solid fuel regresses at the same time. The flame spread rate is determined by tracking the pyrolysis front from the video frame by frame. Figure 6 shows the images of the pyrolysis front spread under air with a flow velocity of 3 cm/s . The measured flame spread rate (V_f) is plotted in Figure 7a. The flame spread rate is almost a constant after the ignition indicating that flame spread is in a steady state (see more details in the Appendix). The flame spread rate increases with the concurrent flow velocity, because of a longer flame length and the enhanced convective flame heat flux [5].

A few minutes after ignition, both the fuel regression rate and flame spread rate will become constant when a fixed regression angle is formed (see Figure 3a) [39]. Normally, from 20-mm away from the ignition zone, the shape of the regression surface and the rate of regression become steady. To measure the rate of regression, two thermocouples located 1 mm and 3 mm below the surface were used to measure the regression rate (r_s). Note that under a lower oxygen concentration, the single flamelet shrinks towards the center (see Figure 4), and partial regression occurs (Figure 3c), where only a thin surface layer and central part of PMMA are burnt. Thus, in some cases, the thermocouple beads near the side (see Figure 1) can no longer track the real-time regression in some experiments.

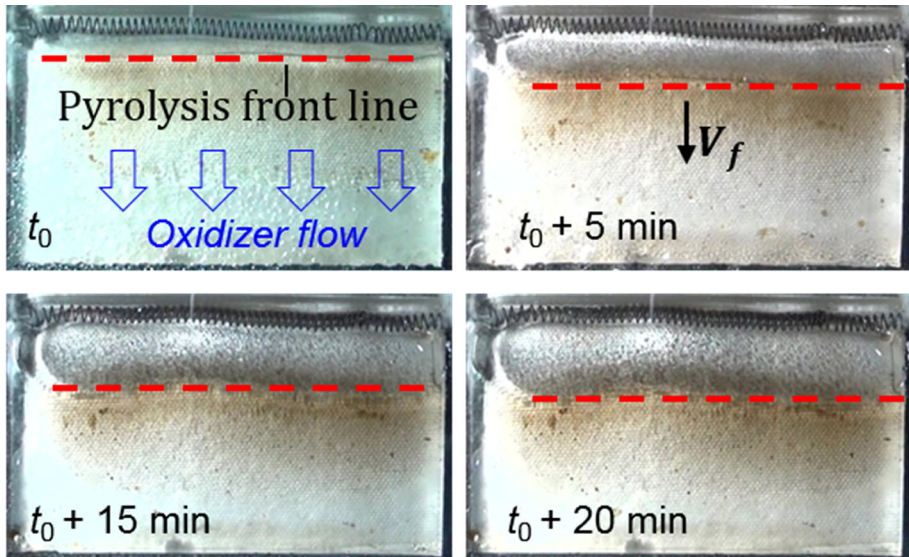


Figure 6. Images of the pyrolysis front spread under air with a flow velocity of 3 cm/s .

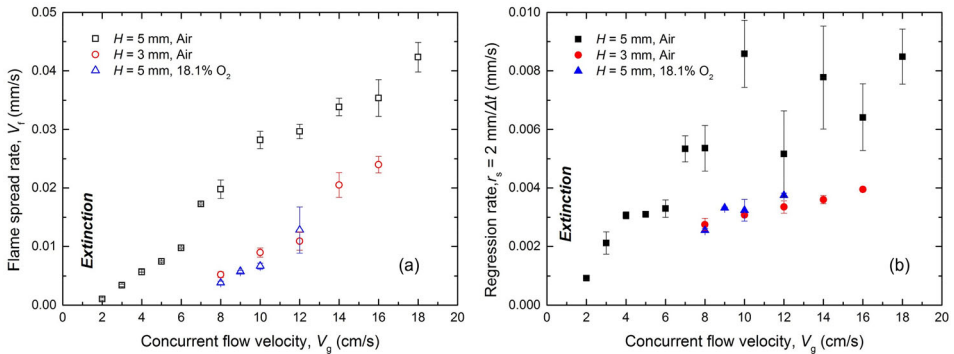


Figure 7. Rates of flame spread rate (a) and fuel regression (b) under varying concurrent airflow and oxygen concentration.

The variations of the temperature at the position of 3 mm below the surface at different oxidizer flow velocities are shown in Figure 8. By tracking the moment of pyrolysis at different depths, the regression rate is calculated. In this work, it is assumed that the pyrolysis temperature is constant at all the concentrations and flow velocities. It is, however, difficult to measure the regression rate precisely because the variation of oxygen concentration and flow velocity could play a role in changing the pyrolysis temperature, even if these effects are small. Figure 7b plots the regression rate as a function of the concurrent flow velocity that is compared with the flame spread rate. Clearly, the regression rate also increases with the concurrent flow velocity. Referring to the opposed flame spread [37, 39], the relationship between the flame spread rate (V_f) and the regression rate (r_s) is

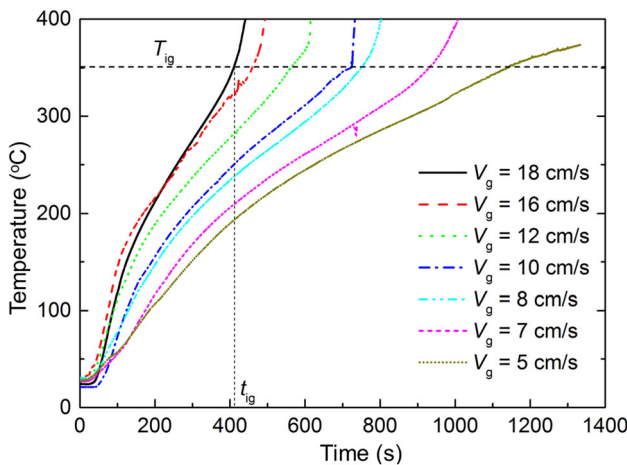


Figure 8. Variation of the solid temperature at the position of 3 mm beneath the sample surface with time under different flow velocities.

$$r_s = V_f \sin\theta \tag{1}$$

where θ is the regression angle (see Figure 3). This relationship supports that both the flame spread rate and regression rate reach the steady state, even when the oxygen supply is very limited.

Figure 9 further summarizes the regression angle vs. the oxidizer flow rate and oxygen concentration. In the *Flame-Spread Regime*, it is found that the regression angle is small ($< 30^\circ$) and gradually decreases with the increasing concurrent flow. Eventually, the regression angle approaches about 10° , when the flame becomes more intense. However, in the low-flow *Fuel-Regression Regime*, the flame is almost standup or even tilted upstream, so the regression angle increases significantly as the flow velocity decreases. Eventually, the fuel-regression surface has a shape that is close to vertical ($\theta \rightarrow 90^\circ$, $\sin\theta \rightarrow 1$), where Equation (1) is still valid, as the rate of fuel regression almost equals to rate of flame motion ($r_s \approx V_f$). Note that flame no longer spreads under extremely limited oxygen supply, (1) the flame is not strong enough to heat the downstream fuel, and (2) there is no oxygen downstream the flame to cause a piloted ignition.

4. Discussion

4.1. Global Flame Equivalence Ratio

For the flame spreading over solid fuel, it is a diffusive flame in nature, so the mixing of the pyrolysis fuel and the oxidizer is important for the spreading pro-

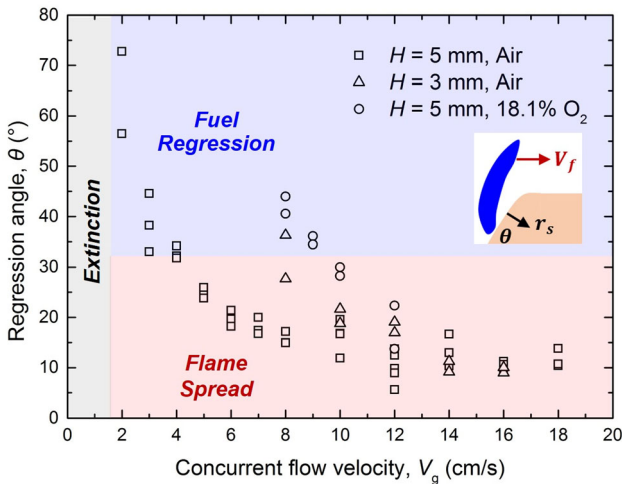


Figure 9. The calculated regression angle (θ) under varying concurrent airflow and oxygen concentration.

cess. Considering that the oxidizer flow is confined in the channel, the overall stoichiometry of a spreading flame can be transparently defined.

In terms of mass conservation, the mass feed rate of fuel from the sample in the flame-fixed coordinates is global flame equivalence ratio Φ (fuel-to-oxygen feed ratio normalized by its stoichiometric value (F/O)) can be written as

$$\phi = \frac{\dot{m}_f}{\dot{m}_g} \frac{1}{(F/O)_{st}} \quad (2)$$

where \dot{m}_f is the mass feed rate of fuel from the sample, \dot{m}_g is the mass flow rate of oxidizer flow. The fuel-to-oxygen mass stoichiometric ratio for PMMA ($C_5H_8O_2$) has a fixed value of 0.52, see Table 1. For the concurrent spread flame, \dot{m}_f can be calculated by the regression rate, and

$$\dot{m}_f = \rho_f r_s L W \quad (3)$$

where ρ_f and r_s are the density and regression rate of the fuel, $L = 20$ mm is the distance between the upper side of the sample and the thermocouple, and W is the flame width. The value of \dot{m}_g can be calculated as

$$\dot{m}_g = \rho_g V_g H W Y_{O_2} \quad (4)$$

where ρ_g is the gas density, V_g is the concurrent flow velocity, H is the channel height.

The calculated overall equivalence ratio (ϕ) as a function of concurrent flow velocity is shown in Figure 10. The equivalence ratio is generally a monotonically decreasing function of the gas flow rate, which is in accordance with the opposed flow spread mode [24]. As expected, the overall combustion stoichiometry becomes richer as the flow velocity decreases. For the near-limit flame spread, the overall global flame equivalence ratio inside the channel is much higher than 1, indicating the flame inside is oxygen-limited.

Further reducing the flow velocity, the oxygen concentration, or the channel height, the equivalence ratio (ϕ) increases dramatically above 1.9, indicating the transition from concurrent flame spread to fuel-regression mode. Eventually,

Table 1
Parameter Values Used for Calculations

Quantity (Units)	Value
Fuel density (kg/m^3)	1190
Fuel width (mm)	100
Fuel molecular weight (kg/mol)	100
Stoichiometric fuel to oxygen mass ratio (–)	0.52
Oxidizer density (kg/m^3)	1.18

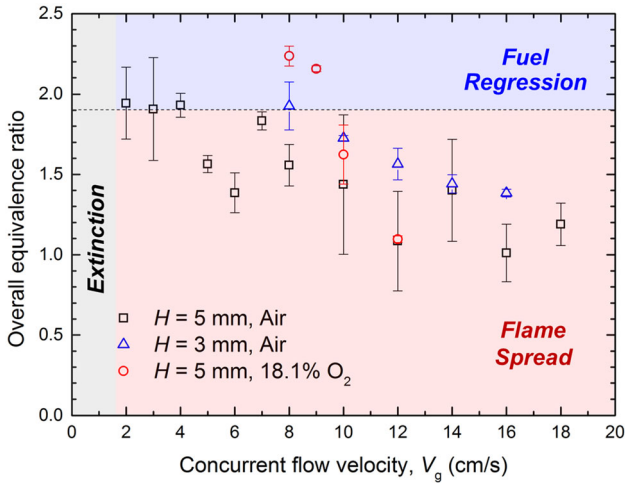


Figure 10. Overall equivalence ratio (ϕ) as a function of concurrent oxidizer flow velocity.

extinction occurs when the equivalence ratio is much higher than 2. The value for the extinction limit cannot be determined exactly because the rates of flame spread and regression cannot be measured in the extinction cases.

In addition to the overall equivalence ratio, the premixed length in the premixed flame should be considered. For a near-limit diffusion flame, the premixed region where the pyrolyzed fuel is mixed with the oxidizer flow (i.e., the triple flame [43]) becomes more important. For a concurrent flame, the mass flux of the pyrolysis products is highest at the base of the flame [3]. At the upstream of the flame tip, the pyrolysis fuel gas is too rich to burn, as it does not have sufficient mixing time. Thus, it has to move along with the oxygen downstream to reach the rich flammability limit. Besides, due to the effect of the side oxygen diffusion, the downstream flame has a higher chance of surviving with an additional side oxidizer supply (or the three-dimensional effect).

4.2. “Round-Trip” Flame Phenomenon

For near-limit flame spread over solid fuel, both opposed and concurrent flame spread processes could occur in the narrow channel environment. For opposed spread, the forward heat conduction from the flame leading-edge to the solid dominates the flame spread process, where most of the heat transfers downstream that is not used to heat the unburned fuel. In contrast, for the concurrent spread, the convective heat from the gas phase is transferred downstream to the unburned fuel, which is a more effective use of flame heating. Moreover, because of the existence of the fuel-regression mode, given a low oxidizer flow, the flame becomes more difficult to extinguish in the concurrent flow than in the opposed flow. Thus, the near-limit flame in the opposed flow tends to transition to a more stable form

in the concurrent flow. This section shows a “round trip” flame phenomenon (first opposed spread, then concurrent burning) to support such a tendency.

In the opposed flow, the near-limit flame only quickly spreads over the surface of the solid without burning out the fuel [32, 33]. Therefore, when the opposed flame spread reaches the end of fuel, most of the fuel still remains to sustain the flame. The “round-trip” experiments were carried by moving the igniter to the downstream of the fuel. Figure 11 shows a flame-spread process initially in the opposed airflow. As a result, the flame will transition to the fuel-regression mode in the concurrent flow until the whole fuel burns out, showing a “round trip” flame phenomenon. Such a phenomenon will occur as long as the oxygen supply is limited for the opposed flame spread, because there is no extra oxygen leaking through the flame to burn the solid fuel.

In other words, there are two stages: the opposed flame spread in Stage 1 and the concurrent fuel regression in Stage 2. In Stage 1, the flame shows a crescent-moon shape, where the middle part of the leading edge is slightly faster than the side part, and most fuel is left. When the flame reaches the end of the fuel sample, the flame leading edge or the fuel-regression front becomes flatter, moving forward in the concurrent flow in Stage 2, where more soot yield is observed. Moreover, similar “round-trip” phenomena have also been observed in smoldering fire spread in porous peat [44] and glowing propagation on the char-particle bed [45]. Thus, “round-trip” or two-stage burning is a common combustion phenomenon in an oxygen-limited environment.

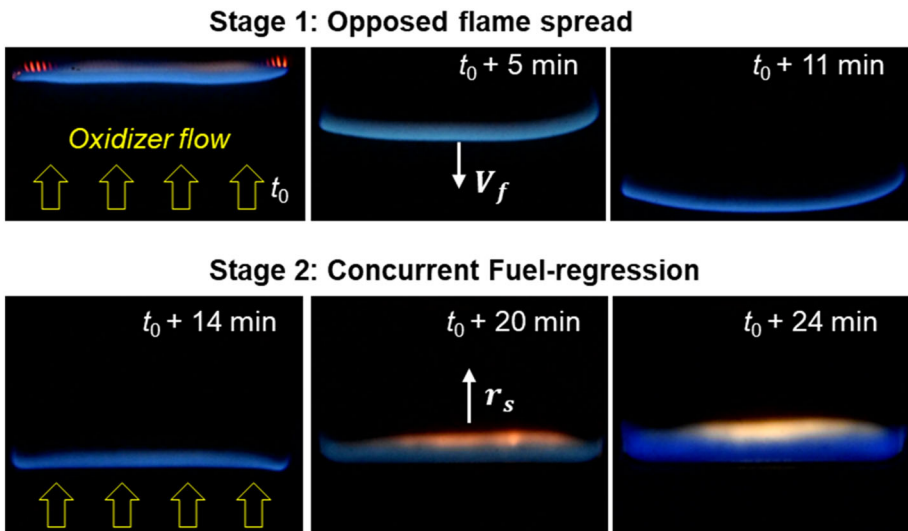


Figure 11. Two-stage “round-trip” flame spread in the air with a flow velocity of 10 cm/s (Video S3).

5. Conclusions

In this study, the oxygen-limited concurrent flame spread over thermally thick solid fuel has been investigated by employing a narrow channel apparatus. As the concurrent flow velocity and oxygen concentration decrease, the conventional concurrent flame spread will transition to the fuel-regression mode, which burns and moves like a candle flame. Further reducing the oxygen supply, the flame tilts towards the inflow, which looks like the flame in the opposed flow, and partial fuel regression occurs.

A flammability map is found for three regimes (1) concurrent flame spread, (2) fuel regression, and (3) extinction, which are defined by the oxygen supply (i.e., oxygen concentration and flow velocity). The newly defined fuel-regression regime can be further characterized by a fuel regression angle of over 30° and a global flame equivalence ratio of over 1.9. The existence of the fuel-regression mode extends the low-flow flammability limit in the concurrent flow. Finally, the “round-trip” flame phenomenon is observed where the 1st-stage near-limit opposed flame spread transitions to the 2nd-stage fuel-regression in the concurrent flow. This work provides new insights into concurrent flame-spread and extinction behaviors under oxygen-limited and microgravity environments.

Acknowledgements

This work is supported by the National Key R&D Program of China (Grant No. 2021YFA0716203), the Opening Fund of State Key Laboratory of Fire Science (SKLFS) under Grant No. HZ2021-KF12, and the National Natural Science Foundation of China under Grant No. U1738117.

Declarations

Conflict of interest The authors declare that there is no conflict of interest.

Appendix

The velocity profiles at the outlet of the narrow channel with a height of 5 mm are shown in Figure 12. The gas flow velocity near the wall is about 2 cm/s, slightly slower than that in the central region, mainly due to the effect of the boundary layer. The average velocity is close to the forced flow velocity. In general, it can be considered that the flow field around the sample is uniform.

The position of the pyrolysis front as a function of time is measured at various flow velocities under an air environment, as shown in Figure 13. It is seen that the pyrolysis front has a linear relationship with time, implying that the flame in the concurrent assistant flow environment is in a steady state.

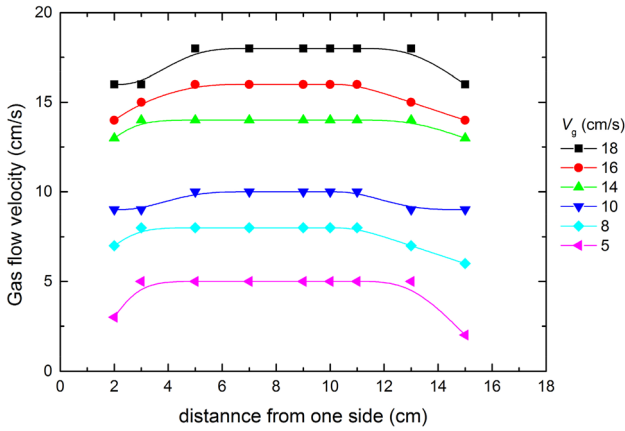


Figure 12. The velocity profile at the outlet of the narrow channel with a height of 5 mm.

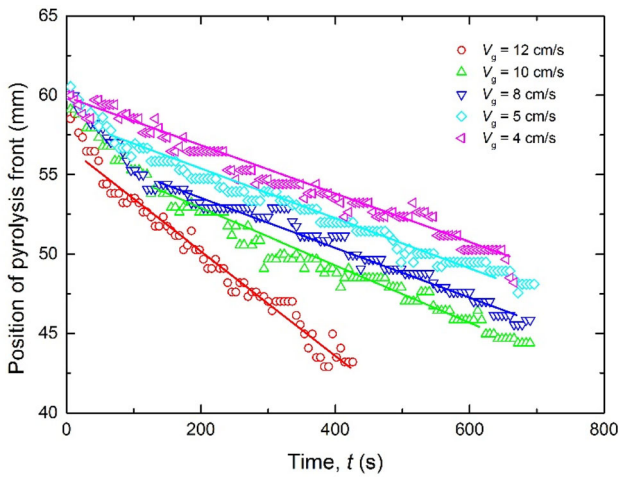


Figure 13. The time evolution of the pyrolysis front position under air with different flow velocities.

Images of flame under 18.1% O_2 with a flow velocity of 8 cm/s from the top view are shown in Figure 14. The time evolution of the flame base position is measured from the top-view images. The yellow line depicts the flame boundary.

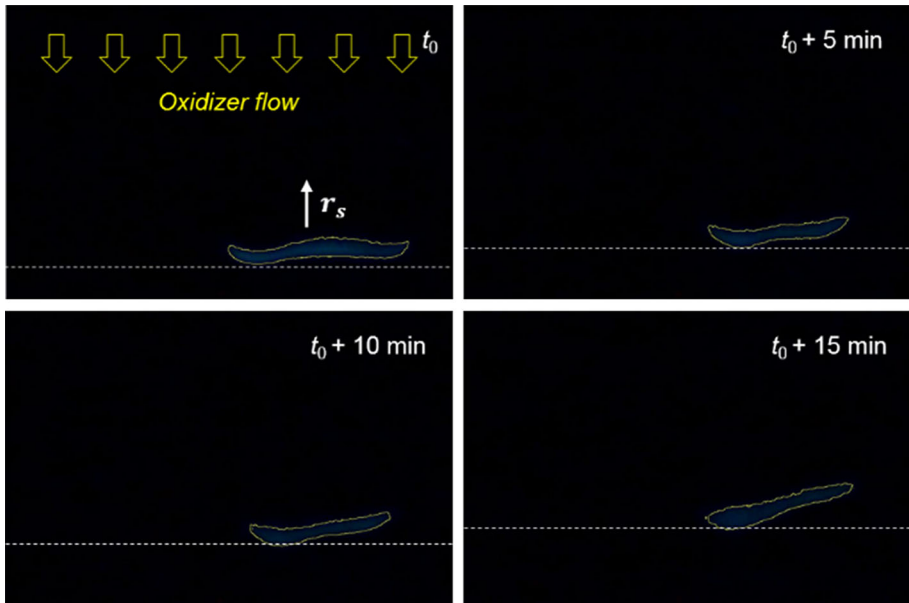


Figure 14. Images of flame spread from top view under 18.1% O₂ with a flow velocity of 8 cm/s. The yellow line depicts the flame boundary.

SUPPLEMENTARY INFORMATION

The online version contains supplementary material available at <https://doi.org/10.1007/s10694-023-01369-9>.

References

1. Williams FA (1977) Mechanisms of fire spread. *Symp Combust* 16:1281–1294
2. Gollner MJ, Miller CH, Tang W, Singh AV (2017) The effect of flow and geometry on concurrent flame spread. *Fire Saf J* 91:68–78
3. T'ien JS, Shih HY, Jiang CB, Ross HD, Miller FJ, Fernandez-Pello AC et al (2001) Mechanisms of flame spread and smolder wave propagation. In: Ross HD (ed) *Microgravity combustion: fire in free fall* Academic Press, Massachusetts, pp 299–418
4. Fernandez-Pello AC (1984) Flame spread modeling. *Combust Sci Technol* 39:119–134
5. Loh HT, Fernandez-Pello AC (1985) A study of the controlling mechanisms of flow assisted flame spread. *Symp Combust* 20:1575–1582
6. Osorio AF, Fernandez-Pello C, Urban DL, Ruff GA (2012) External radiant flux and oxygen concentration as conditions for concurrent flame spread in fabrics. *42nd International Conference on Environmental Systems* 2012:3538
7. Thomsen M, Fernandez-Pello C, Ruff GA, Urban DL (2019) Buoyancy effects on concurrent flame spread over thick PMMA. *Combust Flame* 199:279–291
8. Zhou L, Fernandez-Pello AC (1991) Concurrent turbulent flame spread. *Symp Combust* 23:1709–1714

9. Zhu F, Lu Z, Wang S (2016) Flame spread and extinction over a thick solid fuel in low-velocity opposed and concurrent flows. *Microgravity Sci Technol* 28:87–94
10. Thomsen M, Huang X, Fernandez-Pello C, Urban DL, Ruff GA (2019) Concurrent flame spread over externally heated Nomex under mixed convection flow. *Proc Combust Inst* 37: 3801–3808
11. Thomsen M, Fernandez-Pello C, Urban DL, Ruff GA, Olson SL (2019) On simulating concurrent flame spread in reduced gravity by reducing ambient pressure. *Proc Combust Inst* 37:3793–3800
12. NASA Technical Standard (1998) Flammability, odor, offgassing, and compatibility requirements and test procedures for materials in environments that support combustion
13. Center ESNEENE space research and technology (2014) Space product assurance - Flammability testing for the screening of space materials. EN 16602–70–21
14. ISO 11925–2 (2002) Reaction to fire tests-Ignitability of building products subjected to direct impingement of flame-Part 2: Single-flame source test
15. Zhu N, Huang X, Fang J, Yang L, Hu L (2021) Transitional flame-spread and fuel-regression behaviors under the change of concurrent wind. *Fire Saf J* 120:103015
16. Olson SL, Ferkul PV, Marcum JW (2019) High-speed video analysis of flame oscillations along a PMMA rod after stagnation region blowoff. *Proc Combust Inst* 37:1555–1562
17. Marcum JW, Ferkul PV, Olson SL (2019) PMMA rod stagnation region flame blowoff limits at various radii, oxygen concentrations, and mixed stretch rates. *Proc Combust Inst* 37:4001–4008
18. Tseng Y-T, Tien JS (2010) Limiting length, steady spread, and nongrowing flames in concurrent flow over solids. *J Heat Transfer* 132:091201
19. Olson SL, Ruff GA, Ferkul PV, Owens JC, Easton J, Liao YT, et al (2023) The effect of duct size, sample size, and fuel composition on concurrent flame spread over large cellulose samples in microgravity. *Combust Flame* 248:112559
20. Urban DL, Ferkul P, Olson S, Ruff GA, Easton J, T'ien JS et al (2019) Flame spread: effects of microgravity and scale. *Combust Flame* 199:168–182
21. Ivanov AV, Balashov YV, Andreeva TV, Melikhov AS (1999) Experimental Flammability Verification in Space of Material NASA/CR-1999–209405
22. Olson SL, Miller FJ, Jahangirian S, Wichman IS (2009) Flame spread over thin fuels in actual and simulated microgravity conditions. *Combust Flame* 156:1214–1226
23. Zhang X, Yu Y (2011) Experimental studies on the three-dimensional effects of opposed-flow flame spread over thin solid materials. *Combust Flame* 158:1193–1200
24. Hossain S, Wichman IS, Sidebotham GW, Olson SL, Miller FJ (2018) Influence of gap height and flow field on global stoichiometry and heat losses during opposed flow flame spread over thin fuels in simulated microgravity. *Combust Flame* 193:133–144
25. Hossain S, Wichman IS, Miller FJ, Olson SL (2020) Opposed flow flame spread over thermally thick solid fuels: buoyant flow suppression, stretch rate theory, and the regressive burning regime. *Combust Flame* 219:57–69
26. Zhu F, Wang S, Lu Z (2018) A comparative study of near-limit flame spread over a thick solid in space- and ground-based experiments. *Microgravity Sci Technol* 30:943–949
27. Zhu F, Wang S, Lu Z, Wu C (2021) Opposed flame spread over thick solid fuels under influence of sub-atmospheric pressure and low-velocity flow. *Fire Saf J* 125:103430
28. Vetturini A, Cui W, Liao YT, Olson S, Ferkul P (2020) Flame spread over ultra-thin solids: effect of area density and concurrent-opposed spread reversal phenomenon. *Fire Technol* 56:91–111

29. Olson SL, Miller FJ (2009) Experimental comparison of opposed and concurrent flame spread in a forced convective microgravity environment. *Proc Combust Inst* 32:2445–2452
30. Zhu F, Lu Z, Wang S, Yin Y (2019) Microgravity diffusion flame spread over a thick solid in step-changed low-velocity opposed flows. *Combust Flame* 205:55–67
31. Zhou S, Qi X, Gao J, Huang X, Zhang D (2022) Countercurrent flame propagation and quenching behaviour in a packed bed of spherical PMMA beads in an upward flow of pure oxygen. *Combust Sci Technol* (in press)
32. Matsuoka T, Nakashima K, Nakamura Y, Noda S (2017) Appearance of flamelets spreading over thermally thick fuel. *Proc Combust Inst* 36:3019–3026
33. Wang SF, Zhu F, Lu ZB (2016) Near-limit flame spread over thick solid fuels. *J Combust Sci Technol* 22:402–407
34. Wang S, Wang S, Zhu K, Xiao Y, Lu Z (2016) Near quenching limit instabilities of concurrent flame spread over thin solid fuel. *Combust Sci Technol* 188:451–471
35. Olson SL, Urban DL, Ruff GA, Ferkul PV, Toth B, Eigenbrod C et al (2020) Concurrent flame spread over two-sided thick PMMA Slabs in microgravity. *Fire Technol* 56:49–69
36. Jiang L, He JJ, Sun JH (2018) Sample width and thickness effects on upward flame spread over PMMA surface. *J Hazard Mater* 342:114–120
37. Huang X, Link S, Rodriguez A, Thomsen M, Olson S, Ferkul P, et al (2019) Transition from opposed flame spread to fuel regression and blow off: Effect of flow, atmosphere, and microgravity. *Proc Combust Inst* 37:4117–4126
38. Olson SL (1991) Mechanisms of microgravity flame spread over a thin solid fuel: oxygen and opposed flow effects. *Combust Sci Technol* 76:233–249
39. Carmignani L, Rhoades B, Bhattacharjee S (2018) Correlation of burning rate with spread rate for downward flame spread over PMMA. *Fire Technol* 54:613–624
40. Thomsen M, Fernandez-Pello C, Huang X, Olson S, Ferkul P (2020) Buoyancy effect on downward flame spread over PMMA cylinders. *Fire Technol* 56:247–269
41. Fujita O (2015) Solid combustion research in microgravity as a basis of fire safety in space. *Proc Combust Inst* 35:2487–2502
42. Kumar A, Shih HY, T'ien JS (2003) A comparison of extinction limits and spreading rates in opposed and concurrent spreading flames over thin solids. *Combust Flame* 132:667–677
43. Lyons KM (2007) Toward an understanding of the stabilization mechanisms of lifted turbulent jet flames: experiments. *Prog Energy Combust Sci* 33:211–231
44. Huang X, Rein G (2019) Upward-and-downward spread of smoldering peat fire. *Proc Combust Inst* 37:4025–4033
45. Gao J, Qi X, Zhang D, Matsuoka T, Nakamura Y (2021) Propagation of glowing combustion front in a packed bed of activated carbon particles and the role of CO oxidation. *Proc Combust Inst* 38:5023–5032

Publisher's Note Springer Nature remains neutral with regard to jurisdictional claims in published maps and institutional affiliations.

Springer Nature or its licensor (e.g. a society or other partner) holds exclusive rights to this article under a publishing agreement with the author(s) or other rightsholder(s); author self-archiving of the accepted manuscript version of this article is solely governed by the terms of such publishing agreement and applicable law.